Experimental investigation on the synchronization characteristics of a pitch-plunge aeroelastic system exhibiting stall flutter

Experimental Investigation on the Synchronization Characteristics of a Pitch-Plunge Aeroelastic System Exhibiting Stall Flutter

Dheeraj Tripathi,[1] R. Shreenivas,[1] Chandan Bose,[2] Sirshendu Mondal,[3] and J. Venkatramani[1]
[1)] *Department of Mechanical Engineering, Shiv Nadar University, 203207, India*
[2)] *School of Engineering, Institute for Energy Systems, University of Edinburgh, Edinburgh EH9 3FB, United Kingdom*
[3)] *Department of Mechanical Engineering, NIT Durgapur, Durgapur 713209, India*

(*Electronic mail: j.venkatramani@snu.edu.in (JV))

(Dated: 17 June 2022)

This study focuses on characterizing the bifurcation scenario and the underlying synchrony behaviour in a nonlinear aeroelastic system under deterministic as well as stochastic inflow conditions. Wind tunnel experiments are carried out for a canonical pitch-plunge aeroelastic system subjected to dynamic stall conditions. The system is observed to undergo a subcritical Hopf bifurcation, giving way to large-amplitude limit cycle oscillations (LCOs) in the stall flutter regime under the deterministic flow conditions. At this condition, we observe intermittent phase synchronization between pitch and plunge modes near the fold point; whereas, synchronization via phase trapping is observed near the Hopf point. Repeating the experiments under stochastic inflow conditions, we observe two different aeroelastic responses; low amplitude noise-induced random oscillations (NIROs) and high amplitude random LCOs (RLCOs) during stall flutter. The present study shows asynchrony between pitch and plunge modes in the NIRO regime. At the onset of RLCOs, asynchrony persists even though the relative phase distribution changes. With the further increase in flow velocity, we observe intermittent phase synchronization in the flutter regime. To the best of the authors' knowledge, this is the first study reporting the experimental evidence of phase synchronization between pitch and plunge modes of an aeroelastic system, which is of great interest to the nonlinear dynamics community. Furthermore, given the ubiquitous presence of stall behaviour and stochasticity in a variety of engineering systems, such as wind turbine blades, helicopter blades, and unmanned aerial vehicles (UAVs), the present findings will be directly beneficial for the efficient design of futuristic aeroelastic systems.

A variety of aeroelastic structures used in engineering applications, such as wind turbine blades, helicopter blades, UAVs, and many more are prone to dynamical instabilities when subjected to nonlinear fluid-structure interaction. A specific form of nonlinearity, commonly observed in these aeroelastic structures, comes from the oncoming unsteady fluid loads due to dynamic stall. The associated bifurcations are complex and often make the system susceptible to instabilities like stall flutter. Especially, the occurrence of the subcritical genre of instabilities can lead to operational perilousness and can be critical from the viewpoint of structural safety. Given the typical presence of two or more dominant structural modes in aeroelastic structures, a description of the physical mechanism that underlies in the bifurcation scenarios can be adeptly described from the vantage of synchronization theory. The present study is geared towards this end. From wind tunnel experiments performed on a NACA 0012 airfoil under deterministic and stochastic flow conditions, we demonstrate bifurcation scenarios that are of interest to the engineering community. In specific, we demonstrate subcritical Hopf bifurcation route to stall flutter under deterministic flow conditions. Further, near the fold point, intermittent phase synchronization between the pitch and plunge modes is observed; whereas, we observe synchronization through phase trapping near the Hopf point. Under stochastic inflow conditions, the transition from low amplitude NIRO to high amplitude RLCOs (during stall flutter) corresponds to a shift from asynchrony to intermittent phase synchronization between the pitch and plunge modes.

I. INTRODUCTION

A plethora of engineering systems, such as aircraft wings, wind turbine blades, helicopter blades, bridge decks, buildings, UAVs, and natural systems, such as vocal-fold physiology, cardiac rhythms, and lung functioning involve the interaction of fluid loads with elastic structures, and hence can be categorized as *fluid-elastic* systems. Notably, these systems comprise diverse nonlinearities, instrumental in triggering a wide variety of dynamical instabilities. Thus, the bifurcation analysis of aeroelastic systems with a proper understanding of the underlying physical mechanisms is of seminal importance in engineering parlance. Of these nonlinear aeroelastic instabilities, perhaps one of the most crucial is the stall flutter[1,2], which may cause the aeroelastic systems to oscillate with high-amplitude LCOs. Stall flutter arises due to aerodynamic nonlinearity in terms of dynamic stall. Dynamic stall is a source of aerodynamic nonlinearity, which is triggered by various events like flow separation, vortex formation, vortex shedding, and flow reattachment. The different stages of dynamic stall events have been experimentally investigated in the literature for a periodically pitching wing[3,4]. Stall flutter,

on the other hand, is typically investigated on freely oscillating airfoils in wind tunnel experiments[5–8].

Identifying the onset of stall flutter along with the underlying physics has been of pivotal concern in the aeroelastic community. Dimitriadis and Li[5] analysed the bifurcation behaviour of a wing undergoing stall flutter and reported the route to stall flutter to be through a subcritical Hopf bifurcation. Poirel *et al.*[7] conducted stall flutter experiments on NACA 0012 airfoil using different frequency ratios (plunge to pitch). Observing the pitch and plunge frequency content, they showed that stall flutter is essentially pitch dominant except at a frequency ratio close to one, where plunge motion drives the pitch motion. Subsequently, they drew an interesting analogy that aeroelastic systems exhibit the frequency lock-in phenomenon akin to vortex-induced vibration systems for frequency ratios close to one. Similar analyses were carried out by Benaissa *et al.*[8] who reported beating phenomenon during frequency lock-in, resulting from the phase shift between pitch and plunge mode. In essence, most of the studies pertaining to stall flutter report highly complex dynamical signatures with varying underlying physics - leaving ample room for further investigations.

Inferring the physical mechanisms behind the complex bifurcation signatures arising due to dynamic stall and stall flutter becomes further elusive due to the stochasticity associated with the oncoming flow. In field conditions, flow-field possesses random fluctuations, which give rise to 'noise-induced' instabilities[9]. These noise-induced instabilities can significantly alter the bifurcation route and the aeroelastic response dynamics[10–13]. It is thus very important to investigate the role of noise on the mode-coupling of aeroelastic systems and to understand the underlying mechanism through which the response dynamics is altered in the presence of the noise. In other words, throwing light on the nature of dynamical transitions occurring under stall conditions for deterministic and stochastic input flow conditions is a needful venture. Addressing this end of the hitherto gap is the prime focus of this paper. Dynamic transitions in nonlinear systems (be it deterministic or stochastic) can be directly correlated with the transitions in relative phases and frequencies between the oscillators and their mutual synchronization[13–16]. Deriving impetus from the same, the present study focuses on experimental investigations on the nonlinear dynamics of stall flutter with and without the input noise, from the viewpoint of synchronization framework.

Synchronization is a well-known nonlinear phenomenon and has been widely reported in different nonlinear dynamical systems, such as cardiorespiratory systems[17], electrochemical oscillators[18,19], electronic circuits[20], thermoacoustics[15,21–24], vortex-induced vibration systems[16,25], and aeroelastic systems[13,26,27]. Synchronization phenomenon can be classified in a variety of forms, such as complete synchronization, lag synchronization, intermittent phase synchronization, imperfect phase synchronization, among others[13,14,28–30]. The response dynamics of such nonlinear dynamical systems show rich bifurcation behaviour with different phase relationships such as phase locking, phase drifting, phase slips[13,14,16,18,27,31] and a switch between in-phase to anti-phase synchronization, known as phase-flip bifurcation[19,20,32]; see Section II for further details.

The synchronization theory was very recently applied for the two degrees-of-freedom (DOF) pitch-plunge aeroelastic systems[13,27]. Raaj *et al.*[13] numerically obtained the responses of a nonlinear aeroelastic system undergoing classical flutter and investigated the role of synchronization in pre- and post-flutter regimes in the presence of noise. They showed that, during classical flutter, the frequencies coalesce via frequency locking, and the intermittent responses are caused by an intermittent phase synchronization between the pitch and plunge modes. Vishal et el.[27] modelled a coupled nonlinear aeroelastic system by incorporating the nonlinearities in structure and the flow. The authors reported that frequency coalescence under linear aerodynamics occurs via a frequency locking mechanism, which is in agreement with that reported by Raaj *et al.*[13]. On the other hand, under nonlinear aerodynamics (dynamic stall conditions), the route to synchronization was reported to be through the suppression of one of the natural dynamical modes. Under coupled interactions between different types of nonlinearities, the authors reported the presence of a phase-locking mechanism at lower speeds which **transits** to the suppression of natural dynamics via a brief period of asynchrony. Both of these studies adopt numerical approaches, and experimental evidence of the same is missing in the literature to the best of the authors' knowledge.

Furthermore, critical questions pertaining to the routes to instability (both in deterministic and stochastic input flows), along with the identification of subcritical regimes have remained unanswered in the hitherto studies. A unified description of these dynamical transitions to instabilities, occurring under stall, therefore remains still elusive. With the ever-growing need for slender structures in a variety of aeroelastic applications ranging from UAVs to wind turbine blades, which are in turn rife with susceptibility to dynamic stall, it is prohibitive to have limited clarity on the routes to dynamical instability. The present study assuages this end of the gap. This study focuses on experimentally investigating the stall-induced responses of a pitch-plunge aeroelastic system from a synchronization framework. To that end, wind tunnel experiments are conducted on a NACA 0012 wing under deterministic (suction) and stochastic (blowing) inflow conditions. The obtained responses from the pitch and plunge modes are analyzed using the synchronization theory. Flutter boundaries are estimated by systematically varying the flow speed. The underlying synchronization characteristics are investigated by evaluating the phase and frequency of the responses using Hilbert and Fourier transforms, respectively.

The organization of the rest of the paper is as follows. Section II provides a brief overview of the necessary concepts in synchronization theory. Section III provides the details of the experimental setup. The results that emerge from experimental investigation and synchronization studies are discussed in Section IV. Finally, the salient outcomes emerging from this study are summarized in Section V.

II. A CURSORY GLANCE INTO SYNCHRONIZATION THEORY

Though the notion of synchronization[33,34] has now been established comprehensively in the dynamical systems literature, a cursory glimpse into the terminologies of synchronization theory in the context of aeroelastic systems is presented here for the sake of completeness. The synchronization of mutually coupled oscillators can occur through two different mechanisms such as phase locking and suppression of natural dynamics[27]. Several oscillators are said to be phase synchronized[29], when their instantaneous phases are seen to be perfectly locked, (*i.e.*, the relative phases remain constant), but the amplitudes are uncorrelated. For synchronized oscillators, if the average relative phase value (RPV) becomes close to 0, it is termed in-phase synchronization; whereas, an average RPV value close to π indicates anti-phase synchronization.

Typically, the presence of synchronization is analyzed by examining the instantaneous phases and the frequency of the interacting oscillators. The instantaneous phases of the oscillations are generally obtained by adopting an analytic signal approach, wherein the analytic signal, $\zeta(t)$, is a complex quantity with the real part being the original signal, $z(t)$ and the imaginary part being its corresponding Hilbert transform (HT)[34] given by

$$z_H(t) = \frac{1}{\pi} P.V. \int_{-\infty}^{\infty} \frac{z(\tau) d\tau}{(t-\tau)}, \tag{1}$$

where *P.V.* is the Cauchy principal value of the integral. Thus, the analytic signal can be written as

$$\zeta(t) = z(t) + i z_H(t) = A(t) e^{i\phi(t)}, \tag{2}$$

where $\phi(t)$ represents the instantaneous phase, and $A(t)$ is the instantaneous amplitude of the signal. Further, to characterize phase synchronization, the phase locking value (PLV) of the responses is also estimated as $PLV = N^{-1} \left| \sum_{j=1}^{N} exp(i \triangle \phi_j) \right|$, where $\triangle \phi_j = \phi_{j,plunge} - \phi_{j,pitch}$ is the instantaneous RPV between the plunge and pitch responses at the j^{th} instant. A perfectly synchronized state gives a PLV of one, while a completely asynchronous state gives a PLV close to zero. The PLV for an imperfect synchronization gives a value between zero and one[13].

Qualitatively, the extent of the mutual synchronization between the oscillators can be best understood from the changes in RPV ($\Delta\phi$) over time. If the oscillators are perfectly synchronized, the RPV becomes constant, representative of 'phase locking'. However, it is often seen for the experimental data that the RPV is fluctuating but bounded in nature[13,15,16] (see Fig. 1(a)). Such bounded but oscillatory RPVs, termed as 'phase trapping'[15], are also representative of synchronization as their corresponding PLV is generally close to one[13,27]. On the contrary, a monotonous increase or decrease in RPV is called 'phase drifting' (see Fig. 1(b)), representative of asynchrony, with the corresponding PLV being close to zero[13,27]. However, in many cases, the PLVs are neither close to zero nor to one. One of the most commonly seen events in this class is intermittent phase synchronization, wherein phase-locked regions are mixed with phase drifting regions (see Fig. 1(c)). Intermittent phase synchronization is accompanied by 'phase slips'[13,14,16], having jumps of integer multiples of 2π. Such phase slips mark an imperfect or weak phase synchronization. Furthermore, perfectly synchronized coupled oscillators can undergo phase slips when noise is added to the systems[13,15,16,18]. Sometimes the state of synchronization between oscillators suddenly changes from in-phase to anti-phase or vice versa with a variation in the coupling parameter. Thus, a phase jump of π in average RPV is observed (see Fig. 1(d)), accompanied by a simultaneous jump in their frequencies. This kind of transition is known as phase flip bifurcation[19,20].

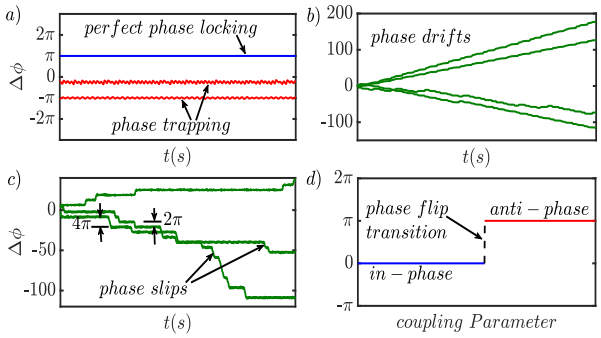

FIG. 1: Schematic representations of different phase synchronization characteristics showing (a) Phase locking/ trapping, (b) phase drifting, (c) intermittent phase synchronization, and (d) phase flip transition.

With these descriptions of the synchronization terminologies, we proceed next to obtain the dynamical signatures, *i.e.* the aeroelastic responses from the wind tunnel experiments. The culmination of instability under nonlinear aerodynamic loading will be cast using the synchronization framework to gain deeper insight into the physics behind the transition to stall flutter under deterministic and stochastic inflow conditions. To that end, details of the experimentation are presented next.

III. EXPERIMENTAL SETUP

The experiments are conducted on a NACA 0012 airfoil having a chord length (c) of 100 mm and a span of 500 mm. The airfoil is mounted horizontally in the low-speed wind tunnel (see Fig. 2(a)) at Shiv Nadar University. The tunnel is capable of operating at a speed of up to 25 m/s and has a test section of dimensions 0.8 m x 0.8 m x 1.2 m. A schematic of the experimental setup inside the wind tunnel test section is shown in Fig. 2(b) and an actual photograph of the setup is also provided in Fig. 2(c). The support mechanism was designed to facilitate two independent degrees-of-freedom for the airfoil motion, namely, pitch and plunge movements and is similar to the ones found in Venkatramani *et al.*[10–12].

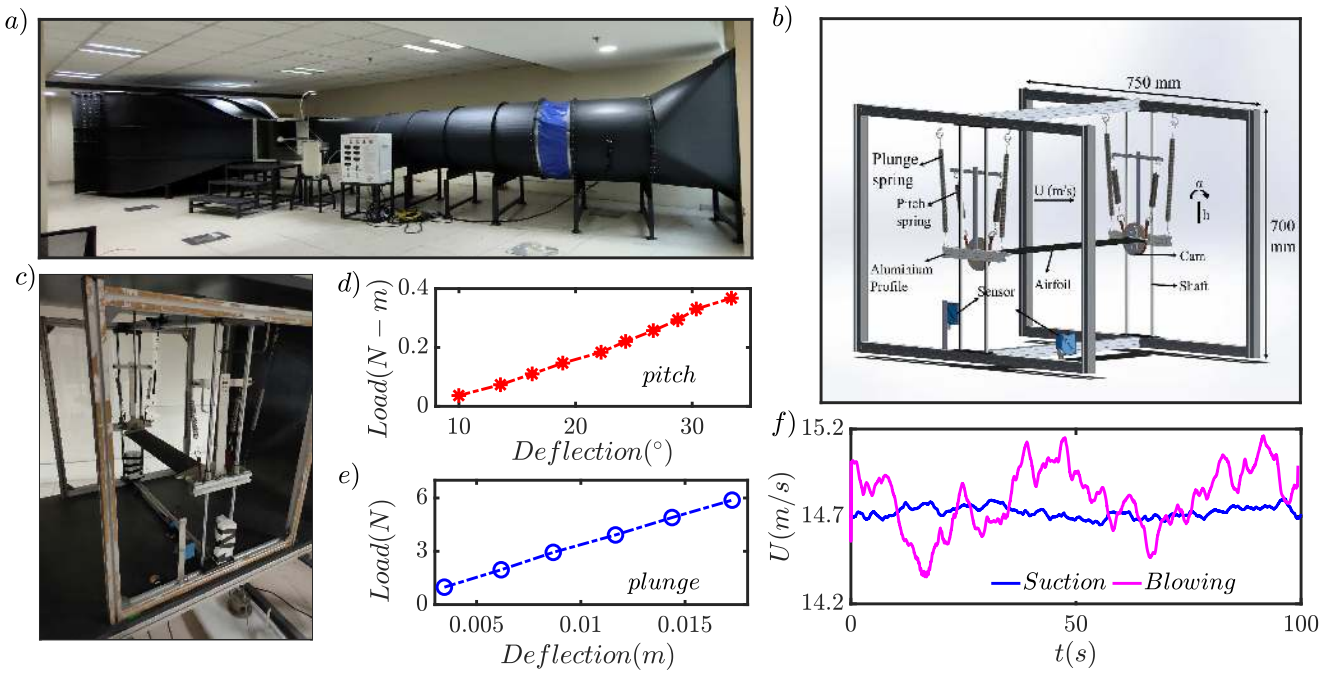

FIG. 2: (a) Photograph of the low-speed closed-section, wind tunnel, (b) schematic depiction of the mechanism that permits pitch-plunge oscillations of the airfoil, (c) photograph of the experimental mechanism. In (d) and (e), the load vs deflection plot for pitch and plunge stiffness respectively are shown. In (f), a sample variation of wind speed with time under suction and blowing conditions is shown.

Restoring force was provided by a pair of tension springs on either side of the airfoil for both pitch and plunge. From the static tests, stiffness in both pitch and plunge springs is found to behave almost linearly (see Figs. 2(d)-(e)). The plunge motion is governed by a translating carriage comprising two shafts that pass through a rectangular aluminium profile via linear ball bushing-guide ways. Rigid hooks are attached to the top frame and the aluminium profile, for attaching plunge springs. The pitching motion of the airfoil is made possible by a pulley-like cam attached to the aluminium profile via a central bearing. The pitch springs are connected to a nylon belt wrapped around the cam.

The motion of the airfoil was measured and recorded by means of two NCDT-type laser displacement sensors having a resolution of 1 micron and a range of 50-350 mm. The sensors were installed below the airfoil, illuminating a spot on the aluminium section and one near the trailing edge. To obtain the plunge displacement, the distance between the lower face of the aluminium section and the elastic axis was measured and added to the sensor reading. A pair of Delta HD 4V3 TS3 type air velocity sensors are used to obtain the flow velocity in the wind tunnel test section. Additionally, a stand-alone hot wire anemometer is used to monitor the flow velocities inside the test section. The signal from the sensors is acquired using an 8-channel Data Acquisition system having a 24-bit resolution.

The wind tunnel is open type and operable in two modes: suction and blowing. In suction mode, the test section is subjected to streamlined flow with minimal fluctuations owing to a honeycomb mesh at the entrance. While in blowing mode, the absence of any mesh gives rise to continuous flow disturbances as the flow enters the test section directly from the fan. Given that the focus of the study involves both deterministic (sterile) and stochastic (fluctuating) flows, we show two sample wind speed time histories for the sake of readers' clarity. As shown in Fig. 2(f), the flow data obtained under suction conditions at speed U = 14.7 m/s is predominantly invariant with time. On the other hand, the flow time history at mean speed U_m = 14.7 m/s measured under blowing conditions shows much higher fluctuations. **Note that, the fluctuation intensity of the noisy input flow in blowing mode changes spatio-temporally as well as with the mean flow speed. However, the variation of fluctuation intensity has not been explicitly reported here, as we feel that the**

TABLE I: Structural parameters for the experiment estimated from static tests.

Parameter	value	description
m_y (kg)	1.908	Total moving mass in plunge
m_α (kg)	0.937	Total moving mass in pitch
f_y (Hz)	2.28	Natural frequency of the plunge mode
f_α (Hz)	4.01	Natural frequency of the pitch mode
x_{EA}	$0.25c$	Position of rotational (elastic) axis from mid-chord
I_α (kg − m^2)	0.0017	Mass moment of inertia in pitch about elastic axis

full information of flow fluctuations in the test section can be best discerned from particle image velocimetry (PIV) - which is currently unavailable with us. The experiments were performed for airspeed in the range of 2-16 m/s, corresponding to the Reynolds number ranging from 1.2 x 10^4 to 1 x 10^5. Table I contains various experimental parameters.

IV. RESULTS AND DISCUSSIONS

A. With deterministic flows

We carry out two isolated methodologies of wind tunnel testing, namely, in suction mode and blowing mode of the fan operation. The latter mode of tunnel fan operation augments flow fluctuations, and the former mode of tunnel fan operation gives rise to largely sterile/deterministic flows. The results and discussions in this subsection are pertaining to the findings obtained from sterile/deterministic flows. The results on stochastic flows are presented in a later subsection.

The initial measurement of airfoil position is taken at zero airspeed to set the reference and subsequently, the wind speed is increased systematically. Under the suction test, two specific forms of experiments are conducted - namely, without and with **an impulsive change** in the initial conditions to the airfoil. **The impulsive change here refers to a manual perturbation to the airfoil to displace it from its initial conditions** - which in turn serves as an avenue to trigger the subcriticality in the aeroelastic system if present.

As a first step, the airspeed is increased without **changing the** initial conditions, and the bifurcation of the response dynamics from a fixed point to sustained high-amplitude LCOs is tracked. Since the above is obtained via an increase in the flow speed, we term the transition of input flow speed from a small value to the critical value as the forward sweep exercise.

Since aeroelastic systems are prone to exhibit subcritical bifurcations, identifying the same in wind tunnel experiments can be pragmatically done by **either providing an impulsive change in initial conditions** to trigger the subcriticality or decreasing the flow speed from the critical value - an exercise termed here as backward sweep. Should LCOs persist even in the backward sweep, subcriticality in the system can be implicitly deciphered[35] (see Fig. 3). In this study, we do both, providing **manual impulsive change in the initial conditions** as well as carrying out a backward sweep to infer the presence of subcriticality. In the methodology involving manual impulse, flow speed in the wind tunnel is increased from zero to critical speed, albeit that a *considerable* initial perturbation is given to the airfoil at each increment of airspeed and the resulting responses are observed. It must be remembered that the need to identify subcritical branches stems from its imminent danger to the structure it poses from operational parlance and the possibility of subcritical bifurcations giving rise to rich synchronization characteristics. The latter will be captured and elaborated on in later parts of this study.

The airfoil response **without perturbing the system from its initial conditions** is plotted against U for pitch (Fig. 3(a)) and plunge (Fig. 3(b)). As U approaches U_{cr}, the response dynamics transforms from a state of rest to large amplitude LCOs, marking the onset of stall flutter instability (see regime-*iii* in Fig. 3(a)). It is worth noting that the presence of large-amplitude pitch oscillations (higher than the stall value for a NACA 0012 airfoil) is one of the reasons to term these large-amplitude LCOs as stall flutter. The other reason is the close match of LCO frequency with the pitch natural frequency of the system. The above two are usually viewed as traditionally established markers for identifying and characterizing stall flutter.

Here, U_{cr} represents the critical flow speed which is $\approx$ 13.7 m/s in our case. Increasing $U > U_{cr}$ results in a considerable increase in the amplitude of LCOs. We refrain from exceeding U too much above the U_{cr}, owing to the practical constraints associated with the experimental framework. Indeed, the pitch amplitudes are high enough ($\approx 35^\circ$) and may possibly jeopardize the setup assembly, hence the maximum flow speed for the forward sweep tests is kept below 16 m/s.

Subsequently, resolving the presence of subcritical dynamics is undertaken. As elaborated earlier, a two-pronged approach is undertaken here. First, we systematically reduce U to the values well below U_{cr} and in turn enable a backward sweep. As shown in Fig. 4, a backward sweep captures the presence of LCOs well below the Hopf point - in specific, till the fold point. In consistent trend with the dynamical systems literature, the amplitudes of the LCOs in the backward sweep reduce as $U < U_{cr}$, and eventually the response dynamics shifts to a fixed point signature at the fold point. Such behaviour is attributed to the presence of subcriticality in the system[35]. One can also trigger the responses to *jump* from the stable, fixed-point regime to stable LCOs, by **changing the initial conditions via manual perturbation** in the proximity of the fold point. It is speculated that a stable fixed point is surrounded by an unstable LCO, which is bounded by a stable LCO as shown in Fig. 4. The lowest airspeed at which the LCOs are observed is approximately U = 9.5 m/s and can be observed in regime-*ii* of Fig. 3(a). Next, an initial condition of $\approx$ 20°, large enough to exceed the static stall angle of NACA 0012[36] is provided **via manual impulse** to the airfoil at different flow speeds. We note that for $U < U_{fld}$, the **manual impulse** merely perturb the response dynamics and culminate in a decaying signature (see inset of regime-*i* of Fig. 3(a)). Note that U_{fld} refers to the fold point as being approximately 9.5 m/s. At $U \geq U_{fld}$, the **manual impulse** trigger the response dynamics to jump to the stable LCO branch and display LCOs (see inset of regime-*ii* of Fig. 3(a)). Larger is the increase in U from the fold point, larger is the amplitude of LCOs; see regimes-*ii* and *iii* shown in Fig. 3(a).

It is clear that there is a coexistence of a stable fixed point attractor (without excitation) and a stable LCO attractor (with excitation) at the flow speeds shown in regime-*ii*. The lowest value of flow speed is approximately the same as the minimum speed at which the LCOs are obtained during the backward sweep experiment and corresponds to the fold point (see schematic in Fig. 4). Though observations of a *jump* to stable LCOs were made in stall flutter experiments by Dimitriadis and Li[5], our study here conclusively demonstrates the presence of a subcritical Hopf bifurcation in aeroelastic systems

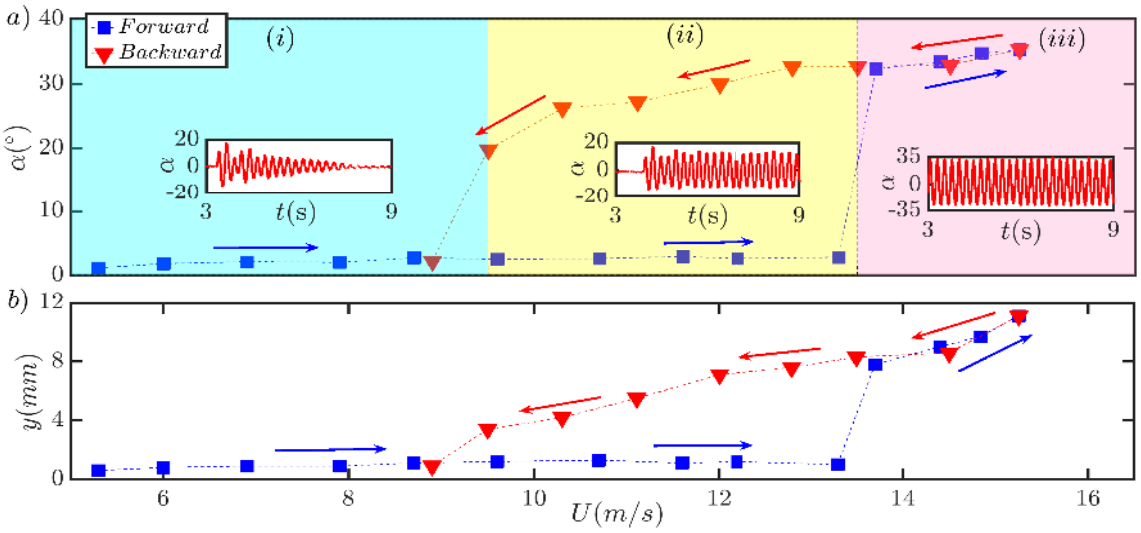

FIG. 3: Bifurcation plots for (a) pitch response, and (b) plunge response, showing the subcritical Hopf bifurcation. Regime (i) shows stable FP attractor, regime (ii) shows coexisting stable FP and stable LCO attractors and regime (iii) shows stable LCO attractor.

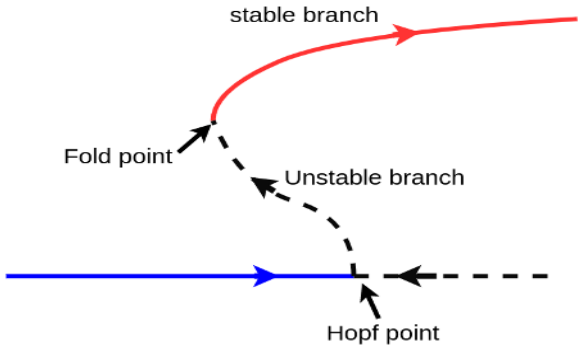

FIG. 4: Schematic of subcritical Hopf followed by fold bifurcation.

undergoing dynamic stall.

Enarmed with the clarity of a subcritical Hopf bifurcation in stall flutter problem, we proceed to investigate the synchronization characteristics. Before embarking on the same, a reiteration of the key findings observed so far is collated here. The present fluid-structure interaction, owing to the physical parameters of the experimental framework, displays large-amplitude LCOs in the pitch DoF. This is possibly indicative of a nonlinear aerodynamic load (dynamic stall) giving rise to large-amplitude LCOs marked by the stall flutter onset. In subsequent sections, we will demonstrate that these oscillations are indeed from a nonlinear aerodynamic loading condition.

The nonlinear aeroelastic system undergoing dynamic stall possesses subcritical characteristics. Sensitivity to initial conditions and the existence of LCOs in the backward sweep are tell-tales of the existence of subcritical behaviour. To discern the physics behind these nonlinear oscillatory signatures, the same is described from the vantage of synchronization theory next.

1. *Dynamic characterization of flutter*

Overall, the pitch LCO amplitudes obtained from suction tests are in the range 18° - 32°. These oscillations are higher than the experimentally reported range of static stall angles[36] and hence possibly are dynamic stall-induced[7,27,37]. To investigate the same, a frequency-based approach is taken up next. Stall flutter is pitch driven and can be experimentally obtained even for a purely pitching airfoil as well and usually, the stall flutter LCO frequency is closer to the pitch natural frequency[37,38].

Route to frequency coalescence is shown in Fig. 5(a) as U increases. For estimating the frequency content below U_{fld}, **it is necessary to offer initial perturbations** and in turn obtain the decaying signatures of the time responses. Once the decaying time responses for $U < U_{fld}$ are obtained, the frequency of the decaying oscillations is evaluated (see Figs. 5(b)-(e)). We observe that with the increase in U, the pitch response frequency remains *almost* invariant, whereas the plunge frequency peak shrinks and coalesces with the pitch frequency as U_{fld} is approached. Indeed, at U_{fld} = 9.5 m/s, pitch and plunge frequencies coalesce *perfectly* at 4.01 Hz which is same as the pitch natural frequency. This feat is usually a strong indicator of stall flutter[5,7,27,37]. **Further increasing the speed above U_{fld}, minimal but gradual increase in coalesced frequency is observed and can be attributed to the increase in positive aerodynamic stiffness and the negative value of aerodynamic damping**[39].

Additionally, below U_{fld}, a secondary peak is also present in both pitch and plunge frequency contents which is very close to the natural frequencies of the other mode (see Fig 5(c) and Fig 5(e)). This is perhaps due to the simultaneous man-

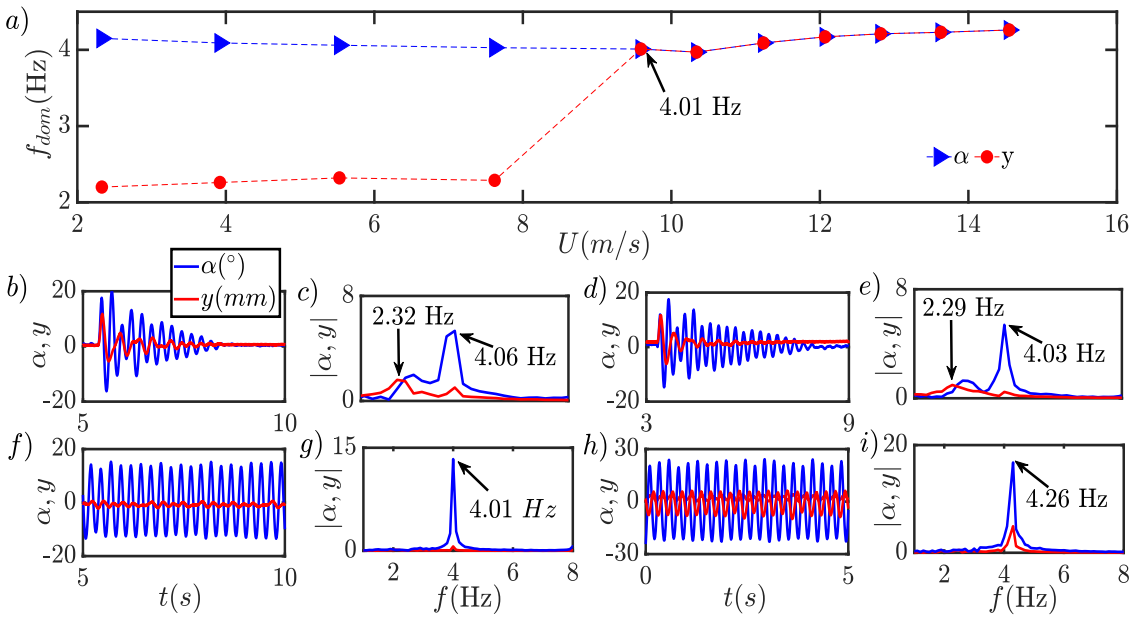

FIG. 5: (a) Variation in the dominant frequency (f_{dom}) of pitch and plunge with U; (b) damped response at U = 5.5 m/s, (c) frequency content at U = 5.5 m/s, (d) damped response at U = 7.6 m/s, (e) frequency content at U = 7.6 m/s, (f) LCO response at U = 9.5 m/s, (g) frequency content at U = 9.5 m/s, (h) LCO response at U = 14.5 m/s, (i) frequency content at U = 14.5 m/s.

ual perturbation given in pitch mode triggering the plunge mode as well[7]. At $U > U_{fld}$ these secondary peaks disappear and only single dominant peak remains near pitch natural frequency (see Fig. 5(g) and Fig. 5(i)). Hence, it is evident that the frequency at flutter onset is pitch dominant and LCOs in Fig. 5(f) and Fig. 5(h) can be characterized as suppression of natural dynamics and is hitherto reported in stall flutter problems addressed numerically[27].

2. *Investigation into synchronization between pitch and plunge mode*

Now we look into the synchronization characteristics of experimentally obtained pitch and plunge responses. Towards this, we simultaneously inspect (i) frequency contents of responses, and (ii) phase difference (RPVs) between pitch and plunge responses. **In Fig. 5(c), Fig. 5(e), Fig. 5(g) and Fig. 5(i), we observe** that the dominant frequency peak of pitch mode is almost stationary and that of the plunge mode gradually shrinks and finally they coalesce near the pitch natural frequency. This mechanism of synchronization is called suppression of natural dynamics and has been reported for the stall-induced aeroelastic systems by Vishal *et al.*[27] using a semi-empirical numerical model albeit experimentally we observe a far closer coalescence of the flutter frequency with the pitch natural frequency in this study.

Next, we analyse the dynamics of RPV ($\Delta\phi$) of pitch and plunge modes. First, we inspect the same in the vicinity of the fold point, U_{fld}. To that end, we obtain the aeroelastic data from the backward sweep experiments. Repeating this exercise for the data generated in the forward sweep with **initial perturbations** gives rise to the same set of findings, and hence are not shown here for the sake of brevity. We observe that at U = 11.1 m/s (see Fig. 6(a)), the RPVs are bounded with minimal fluctuations and has a PLV of 0.95 (see Fig. 6(b)) - which is representative of phase locking between pitch and plunge oscillations. Such bounded fluctuations in RPVs are also characterized as phase trapping[15]. Corresponding radial distribution of relative phase shown in Fig. 6(c) indicates dense RPVs. As the flow speed is decreased to U = 10.3 m/s, the RPVs are still bounded (Fig. 6(a)), however, its radial distribution is visibly more scattered (Fig. 6(d)) and the PLV is reduced to 0.91 (Fig. 6(b)) implying a slight loss in synchronization strength. Further decreasing the flow speed to 9.5 m/s, there is a sudden transition as the RPVs instead of being bounded, undergo phase slips (of integer multiples of 2π). The corresponding PLV is further reduced to approximately 0.85 (Fig. 6(b)) and the radial distribution is highly scattered (Fig. 6(e)) - this indicates the state of intermittent phase synchronization[14]. This regime is closely represented in Fig. 7(a) where the epochs of phase-locking are separated by phase slips (see Fig. 7(b)). This indicates that the instantaneous phases of pitch and plunge are trapped (see Figs. 7(c)-(d)) except for the short duration where the momentary slips jeopardize the phase locking. The flow speed at which phase slip occurs is perhaps the fold point (or close to it) and there is an unstable (LCO) branch associated with it (see Fig. 4). The presence of this unstable branch is possibly the reason that leads to the phenomenon called imperfect phase synchronization with associated phase slips[14]. It is worth mentioning that this point is the minimum value of U for which subcritical LCOs are encountered and for $U < U_{fld}$ the system has only a single attractor *i.e.* the stable fixed point.

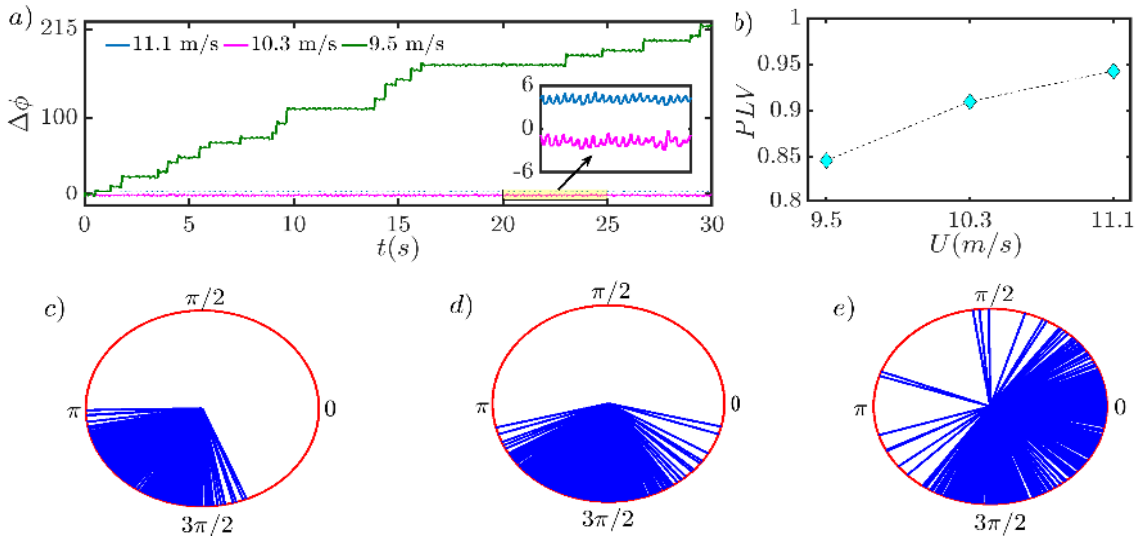

FIG. 6: (a) Time evolution of RPV($\Delta\phi$) near fold point (U = 11.1 - 9.5 m/s); (b) Change in PLV during backward sweep experiment (subcritical stable LCO branch); Radial distribution of $\Delta\phi$ at (c) U = 11.1 m/s, (d) U = 10.3 m/s, and (e) U = 9.5 m/s.

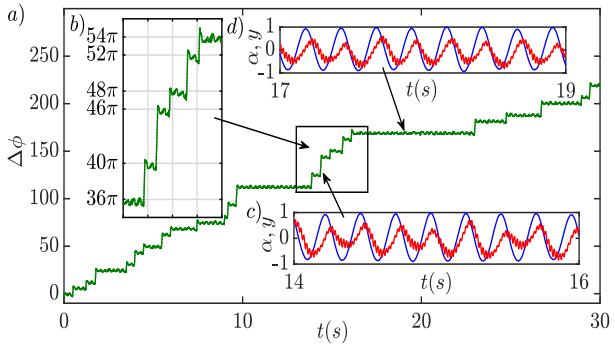

FIG. 7: (a) The phase slips at U = 9.5 m/s (fold point); (b) a closer look at the phase slips shows 2π (or its multiples) jumps. Figures (c)-(d) show normalized pitch-plunge time histories at various instances.

On the other hand, we observe phase synchronization post Hopf point region from the forward sweep experiments. Corresponding RPV and PLV variations are shown in Fig. 8(a) and Fig. 8(b), respectively. At U = 13.7 m/s, the RPVs are bounded but oscillatory in time. The same is also depicted in Fig. 8(c) through the radial variation of RPVs. This represents phase trapping between pitch and plunge modes. As the flow speed is increased to higher values (14.4 m/s - 15.3 m/s), phase trapping (or synchronization) is observed. The radial distribution for U = 14.4 - 15.3 m/s are less scattered (Figs. 8(d)-(f)) compared to that at U = 13.7 m/s, representing a higher coherence between the two oscillators. Corresponding PLVs for the range U = 13.7 - 15.3 m/s are above 0.98 which indicates an occurrence of stronger phase synchronization. The overlapped time histories are shown in Figs. 9(a)-(c) corroborate the same. Note that the frequencies of pitch-plunge oscillators are perfectly coalesced for this range of speeds (see corresponding amplitude spectra in Fig. 9).

In short, stall flutter with large amplitude LCOs corresponds to phase synchronization (through phase trapping) between pitch and plunge modes. The synchronization (or frequency locking) happens through the mechanism known as suppression of natural dynamics (of the plunge mode). Further, near the fold point, intermittent phase synchronization between pitch and plunge modes is observed, wherein the epochs of phase trapping are segregated by the phase slips. Having characterized the synchronization behaviour during the bifurcation to stall flutter with the deterministic flow, we now turn our attention to the same with stochastic inflow conditions.

B. With stochastic flows

In this subsection, the response dynamics of the aeroelastic system under stochastic inflow conditions is obtained and subsequently, the underlying synchronization characteristics of pitch and plunge modes are investigated. The stochastic conditions are provided by the fluctuations in the inflow when the experiments are carried out under the blowing mode.

1. *Dynamic characterization of flutter*

It is observed that the pitch-plunge response dynamics is significantly altered in the presence of noise and we observe small-amplitude NIRO at U_m = 12.8 m/s, even below U_{cr} ($\approx$ 13.7 m/s), as shown in Fig. 10(a). Upon increasing the flow speed above U_{cr} (to U_m = 14.6 m/s), these small-amplitude NIRO persist (see Fig. 10(b)), indicating that the onset of LCOs under stochastic conditions is perhaps delayed. The frequency content of these oscillations shows a broadband

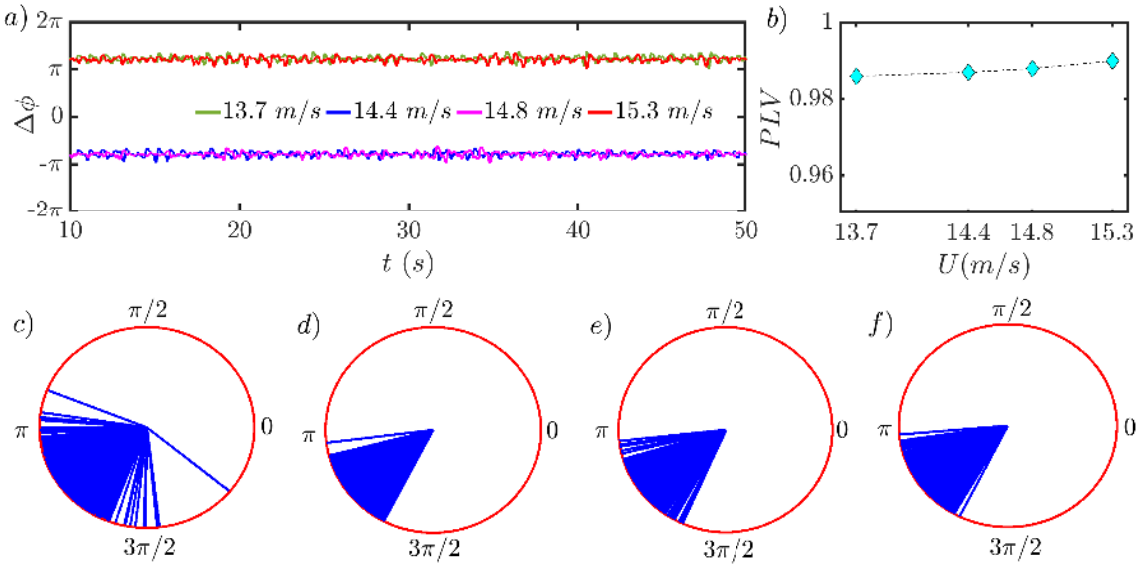

FIG. 8: (a) Time evolution of RPV($\Delta\phi$) post Hopf bifurcation (U = 13.7 - 15.3 m/s); (b) Change in PLV post Hopf point during forward sweep experiment; Radial distribution of $\Delta\phi$ at (c) U = 13.7 m/s, (d) U = 14.4 m/s, (e) U = 14.8 m/s, and (f) U = 15.3 m/s.

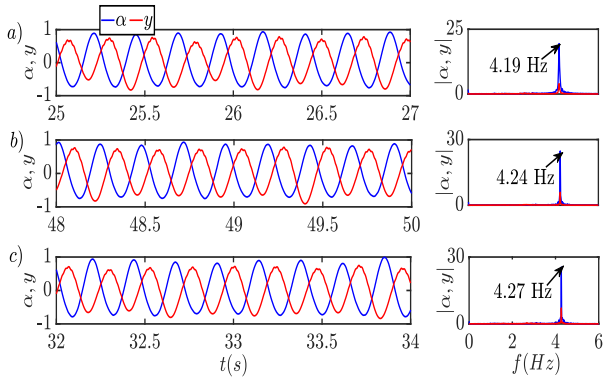

FIG. 9: Sample overlapped time histories of pitch and plunge responses (normalized) and corresponding frequency response post Hopf bifurcation at (a) U = 13.7 m/s, (b) U = 14.8 m/s, and (c) U = 15.3 m/s.

response where multiple frequency peaks are observed (see Figs. 10(a)-(b)) to be concentrated about the respective natural frequencies of pitch and plunge modes. In other words, noise-induced oscillations are observed with some characteristic frequency in the pre-flutter regime.

At U_m = 15.0 m/s, the small amplitude NIRO transforms into large amplitude random LCOs or RLCOs (see Fig. 10(c)). With further increase in flow speed, these RLCOs grow into well-developed LCOs (see Fig. 10(d)). The corresponding frequency response of these RLCOs has a single dominant peak closer to f_α. This implies that the two modes coalesce near f_α resulting in pitch dominant LCOs akin to the deterministic scenario, and hence these LCOs can be termed as stochastic stall flutter[40].

2. *Investigation into synchronization between pitch and plunge mode*

Since the pitch-plunge time histories under fluctuating inflow depict a different class of dynamical signatures than those obtained under deterministic inflow, it is imperative to separately investigate the synchronization characteristics of two modes in a stochastic framework. Akin to the deterministic scenarios shown in Fig. 6 and Fig. 8, an attempt to describe the synchronization characteristics with the bifurcation behaviour was made here. To that end, the temporal evolution of RPVs corresponding to small amplitude NIRO responses are plotted in Fig. 11 and those corresponding to large amplitude RLCO responses are plotted in Fig. 12.

It is observed from Fig. 11(a) that the RPV in the range between U_m = 12.8-14.6 m/s has a random variation with time, where many plateaus of phase-locking amidst phase drifting are observed which denotes asynchrony between the pitch and plunge modes. For clarity, a zoomed section of RPV time histories is shown in Figs. 11(b)-(d). The phase difference does not show a monotonically increasing or decreasing trend over time but rather keeps drifting to a higher or a lower value arbitrarily amidst many phase-trapping epochs. **The NIROs are observed to contain broad band frequency spectrum with multiple dominant peaks (see Fig. 10(a) and Fig. 10(b)) and therefore correlated in nature. For such signals, a perfect asynchrony cannot be expected as there might be some common dominant frequencies. Therefore, the weak phase synchrony observed between pitch and plunge responses in this regime might be due to such common frequency content between pitch and plunge mode**. Figure 12(a) shows the time variation of RPV for U_m = 15.0 - 15.7 m/s, which corresponds to the large amplitude RLCOs

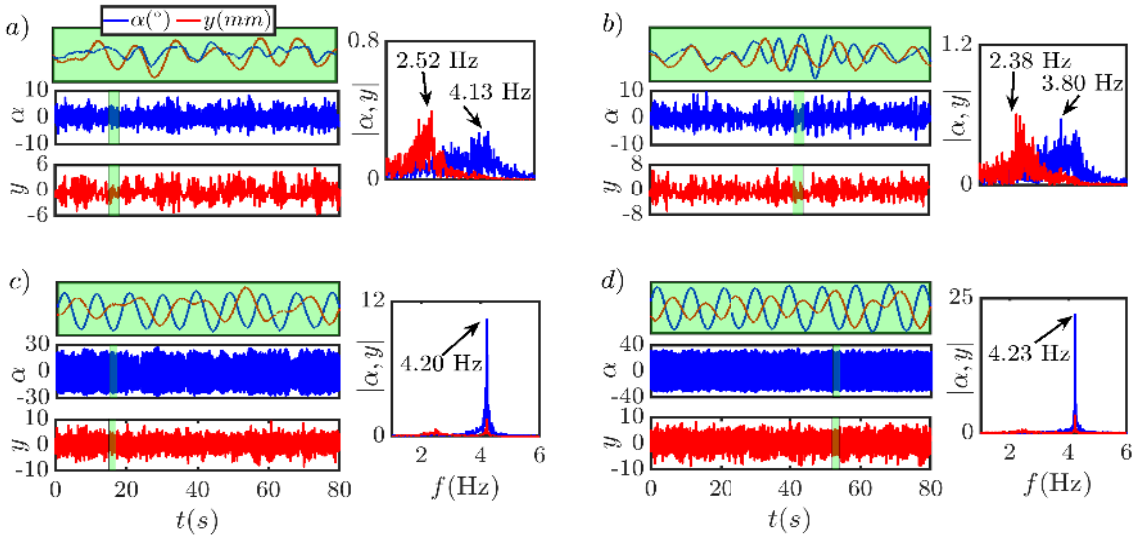

FIG. 10: Aeroelastic response time histories and corresponding frequency response under blowing conditions at (a) U_m = 12.8 m/s, (b) U_m = 14.2 m/s, (c) U_m = 15.0 m/s, and (d) U_m = 15.7 m/s.

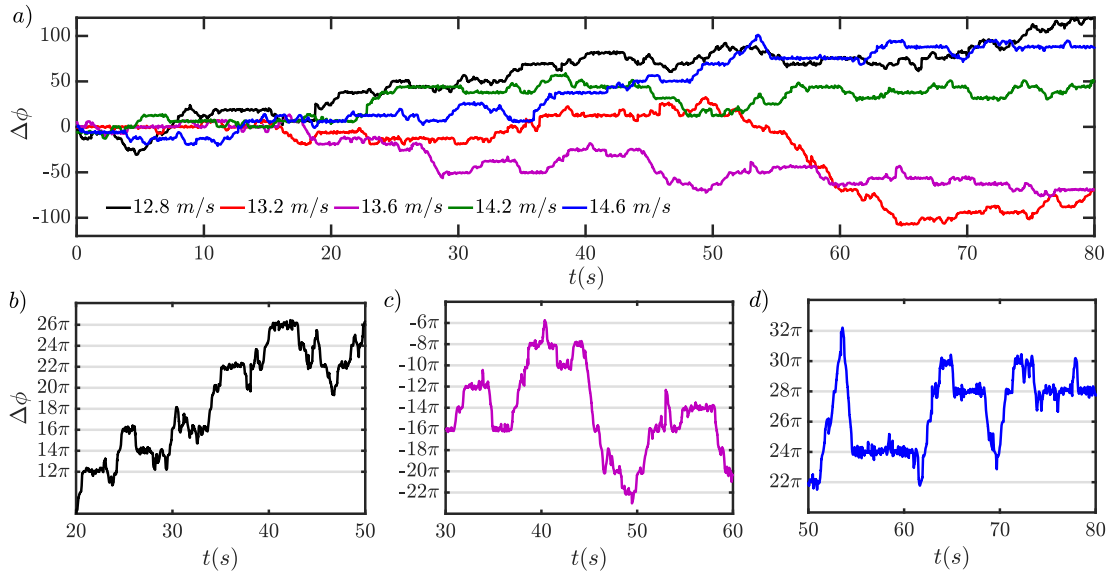

FIG. 11: (a) RPV($\Delta\phi$) time histories under blowing conditions, corresponding to NIROs (before the onset of stochastic stall flutter); a zoomed section of $\Delta\phi$ time history at (b) U_m = 12.8 m/s, (c) U_m = 13.6 m/s, and (d) U_m = 14.6 m/s.

during stochastic stall flutter (see Figs. 10(c)-(d)). At U_m = 15.0 m/s (stochastic bifurcation point), we see a sudden transition in relative phase dynamics as the $\Delta\phi$ monotonously decreases over the time (see Figs. 12(b)-(c)). Here the phase-locking epochs are very short-lived and rarely occurring implying an asynchronous phase dynamics between pitch and plunge modes. On further increasing the flow speed, the appearance of phase-locking epochs becomes more frequent and visibly longer in duration, which is separated by phase slips. Closer looks into the RPVs at U_m = 15.7 m/s for arbitrarily chosen time instances are presented in Figs. 12(d)-(e), which shows multiple phase-locking epochs along with the phase slips (of integer multiples of 2π) indicative of intermittent phase synchronization. Such 2π phase slips are 'noise-enhanced'[13,16,18] and in the absence of noise we encounter the phase trapping characteristics akin to the deterministic case shown in Fig. 8 for this flow speed range. Therefore, in the stochastic stall flutter regime, a transition from asynchrony to intermittent phase synchronization between pitch and plunge modes is observed. With a view to quantifying this transition, we resort to the phase-locking values (PLV) in this flow speed range.

The variation in PLV with mean flow speed is shown in Fig. 13(a), which shows that the PLVs in the stochastic flutter regime ($U_m >$ = 15 m/s) are much lower than those obtained under suction conditions. This indicates that the noise

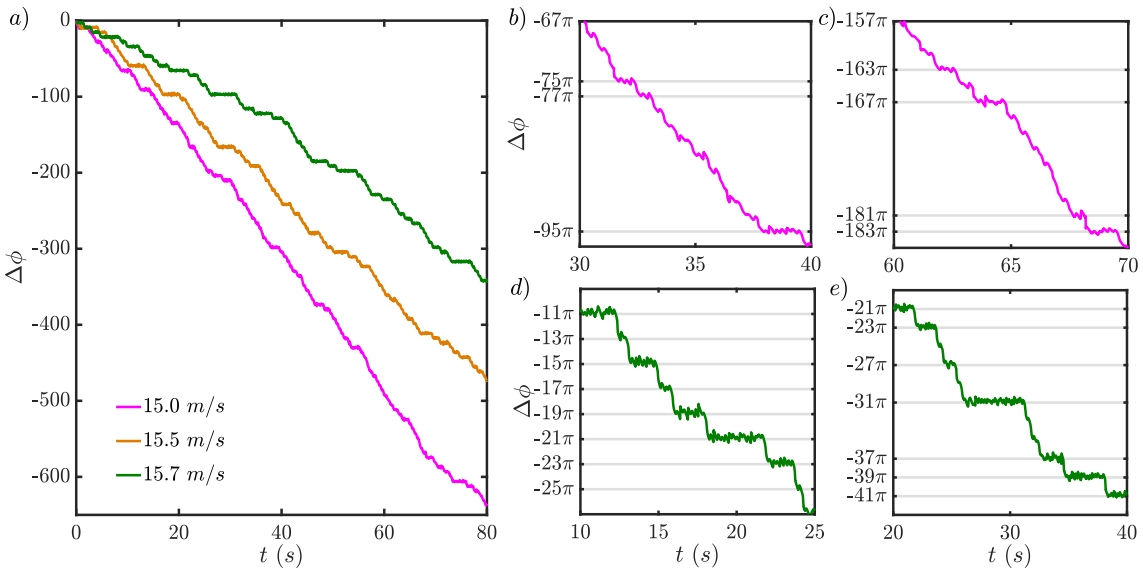

FIG. 12: (a) RPV($\Delta\phi$) time histories under blowing conditions after the onset of high amplitude RLCOs; a zoomed section of $\Delta\phi$ time history at U_m = 15.0 m/s (b)-(c) and 15.7 m/s (d)-(e).

has a significant effect on mutual phase locking between pitch and plunge modes. The PLV at U_m = 12.8 m/s is 0.49 which increases to 0.59 at U_m = 13.2 m/s and subsequently attains approximately a constant value (0.63) between U_m = 13.6 - 14.6 m/s. This is due to the short-lived weak phase locking between pitch and plunge modes observed amidst the overall phase asynchrony (Figs. 13(b)-(d)). At U_m = 15.0 m/s, we see a sudden dip in PLV from 0.63 to 0.57. This justifies the asynchronous phase dynamics with very short-lived and rarely occurring phase-locking epochs observed at the onset of stochastic stall flutter. Upon further increasing the inflow speed up to U_m = 15.7 m/s, PLV gradually increases up to 0.74, quantifying the intermittent phase synchronization in post flutter regime.

Note that, up to U_m = 14.6 m/s, the aeroelastic responses depicts NIRO of small amplitudes which then transition to RLCO at U_m = 15.0 m/s. This transition is highlighted in Fig. 13 and more clearly depicted via stationary joint probability density function (j-pdf) of pitch and its instant derivative (α') in Fig. 13(b) and Fig. 13(c). The topological changes in j-pdf from uni-modal at U_m = 14.6 m/s (representing NIRO) to crater-like structure at U_m = 15.0 m/s (representing RLCOs) are indicative of a stochastic phenomenological or P-bifurcation[41]. However, it is worth noting that the depiction of the stochastic bifurcation points in Fig. 13 is rather based on visual inspections and in turn qualitative. Quantitative measures such as Shannon entropy and Lyapunov exponents[12,41] can offer better insights into the stochastic bifurcations, however, they are beyond the scope of this study.

There are two major differences in relative phase ($\Delta\phi$) dynamics shown in Fig. 11 (corresponding to NIRO) and Fig. 12 (corresponding to RLCOs). First, during NIRO, the RPV is arbitrarily increasing or decreasing over time where noise plays a dominant role in leading to epochs of weak phase locking. While, during RLCO, the RPV monotonically decreases with the intermittent appearance of the phase-locking epochs. The other difference is that although the 2π phase slips are present in both the cases, during NIRO, the average relative phase difference, $\langle\Delta\phi\rangle_t$ during the phase-locking epochs appears to be even multiples of π, while during RLCO, $\langle\Delta\phi\rangle_t$ becomes the odd multiples of π. To understand this more comprehensively, the probability density function (pdf) of RPVs are plotted for the range U_m = 12.8 - 15.7 m/s in Fig. 14. Up to U_m = 14.6 m/s, the pdfs have two peaks one near 0 and the other near 2π, indicating the dominance of in-phase characteristics. At U_m = 15.0 m/s, these two peaks disappear and a single prominent peak is seen near π, indicating the qualitative change in mutual phase synchronization as the phase characteristics are anti-phase. Beyond this flow speed, the peak remains close to π and the synchronization dynamics remain anti-phase.

The point, where the phases transition from in-phase to anti-phase (i.e. U_m = 15.0 m/s) is accompanied by a transition in frequency response as the broadband frequency response transitions to a coalesced single peak (see Fig. 10). The phase jumps of π and a simultaneous jump in frequency in synchronized oscillators is characterized as 'phase flip transition' in-phase synchronization theory[19,20]. The oscillations in this study are not completely synchronized under noise but have a π jump in radial phase distribution and a sudden transition in frequency response simultaneously. More importantly, the transition in phase dynamics occurs at the onset of RLCOs and hence it can be a useful marker for stochastic stall flutter prediction and can be explored further in a separate study.

In short, the transition to stall flutter under stochastic inflow conditions corresponds to the transition from asynchrony with weak phase-locking epochs to intermittent phase synchronization between pitch and plunge modes. Further, a characteristic of phase-flip bifurcation is observed at the onset of RLCOs.

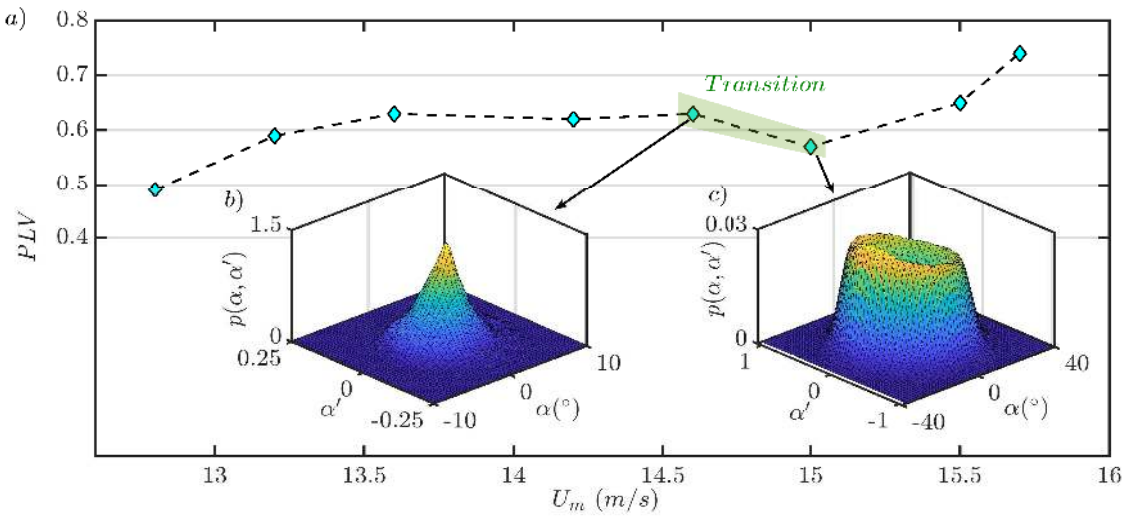

FIG. 13: (a) Variation of PLV of the pitch and plunge responses with flow speed under blowing conditions. The j-pdfs are shown at (b) U_m = 14.6 m/s (corresponding to small amplitude NIROs), and (c) U_m = 15.0 m/s (corresponding to RLCOs) to depict the transition (highlighted) from noise-induced oscillations to stochastic stall flutter.

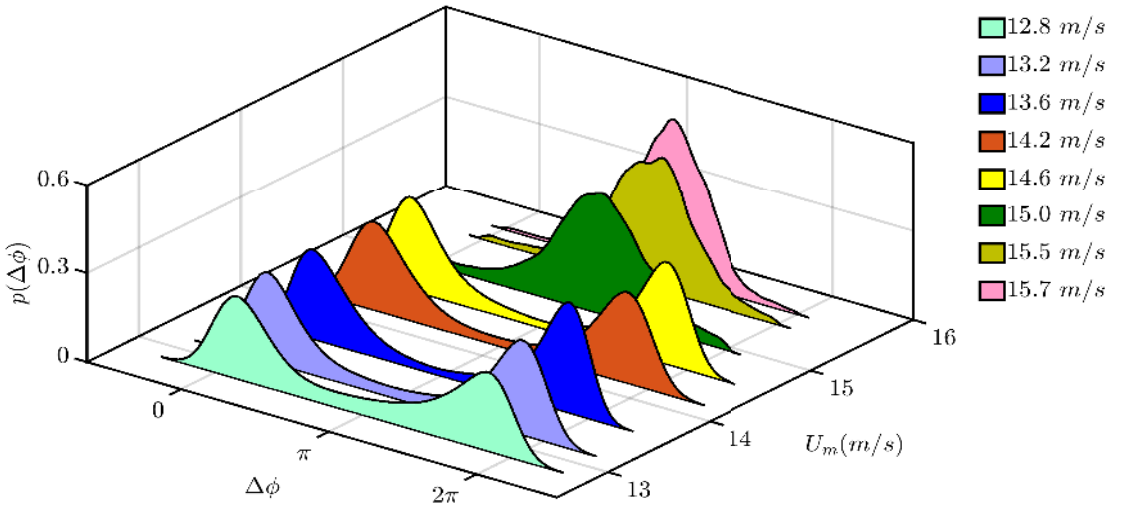

FIG. 14: Cyclic distribution of $\Delta\phi$ depicted via its probability density function. For U_m = 12.8 - 14.6 m/s, two pronounced peaks are observed close to 0 ans 2π (in-phase), respectively. At U_m = 15.0 m/s, a single pronounced peak is observed close to π (anti-phase) and remains as such for U_m = 15.5 m/s and 15.7 m/s.

In wake of recent findings by Tripathi *et al.*[1], that the fatigue damage in nonlinear aeroelastic systems is the highest under the dynamic stall, the present insights towards characterizing stall-induced dynamical signatures can be potentially relevant in the design of futuristic nonlinear aeroelastic systems.

V. CONCLUDING REMARKS

This study presents the physical mechanism of the stall-induced instabilities in the aeroelastic systems through a synchronization framework. The passive pitch and plunge responses of the NACA 0012 foil are measured from wind tunnel experiments under deterministic (suction) and stochastic (blowing) inflow conditions. The aeroelastic system is found to be sensitive to initial conditions due to the presence of co-existing attractors through a subcritical Hopf bifurcation. The frequency response analysis shows that the dominant pitch and plunge frequencies coalesce via the suppression of plunge mode by the pitch mode. Under deterministic inflow conditions, we observe intermittent phase synchronization with phase slips near the fold point; whereas, near the Hopf point, we observe synchronization via phase trapping.

The study is further extended to understand the underlying

synchronization mechanism that gives rise to noise-induced instabilities. Blowing conditions provide higher turbulent intensity, enabling the stochastic scenario with inflow acting as input noise. Consequently, the response dynamics was seen to be very distinct from those under suction conditions. The bifurcation route is altered and the small amplitude NIROs are seen to presage the RLCOs during stall flutter. The role of noise is crucial in altering aeroelastic responses and is well understood from the RPV and PLV observations. The arbitrary phase slips owing to the noise explain the presence of small amplitude NIRO prior to the onset of stochastic stall flutter. Post the stochastic stall flutter onset, noise jeopardizes the phase-locking and we observe intermittent phase synchronization. At the stochastic bifurcation point, changes in the distribution of RPV are observed, as the dominant peaks of RPV become anti-phase from in-phase, a characteristic of phase-flip bifurcation.

This study is perhaps the first to invoke the synchronization theory for experimentally observed stall flutter responses and to provide insights into the transitions in mutual synchronization that take place when the wing undergoes stall flutter, NIRO, and RLCO. The findings presented here can be further extended for developing precursors (via time series analysis[10] or machine learning algorithms[42]) for various aeroelastic instabilities by examining synchronization mechanisms of other nonlinear aeroelastic systems possessing complex response dynamics such as period-doubling and chaos.

DATA AVAILABILITY

The data that support the findings of this study are available from the corresponding author upon reasonable request.

ACKNOWLEDGMENT

The last author is immensely grateful for the financial supports from SERB start-up research grant (SRG/2019/000077) for this research work.

REFERENCES

[1] D. Tripathi, S. Vishal, C. Bose, and J. Venkatramani, International Journal of Non-Linear Mechanics , 104003 (2022).
[2] S. Vishal, A. Raaj, C. Bose, J. Venkatramani, and G. Dimitriadis, Nonlinear Dynamics , 1 (2022).
[3] W. J. McCroskey, L. W. Carr, and K. W. McAlister, Aiaa Journal **14**, 57 (1976).
[4] K. McAlister, S. Pucci, W. McCroskey, and L. Carr, *An Experimental Study of Dynamic Stall on Advanced Airfoil Sections. Volume 2. Pressure and Force Data*, Tech. Rep. (NASA. TM 84245, 1982).
[5] G. Dimitriadis and J. Li, AIAA journal **47**, 2577 (2009).
[6] N. A. Razak, T. Andrianne, and G. Dimitriadis, AIAA journal **49**, 2258 (2011).
[7] D. Poirel, L. Goyaniuk, and A. Benaissa, Journal of Fluids and Structures **79**, 14 (2018).
[8] A. Benaissa, S. Biskri, L. Goyaniuk, D. Poirel, and N. N. Bouda, Journal of Fluids and Structures **100**, 103176 (2021).
[9] Q. Liu, Y. Xu, J. Kurths, and X. Liu, Chaos: An Interdisciplinary Journal of Nonlinear Science **32**, 062101 (2022).
[10] J. Venkatramani, V. Nair, R. Sujith, S. Gupta, and S. Sarkar, Journal of Fluids and Structures **61**, 376 (2016).
[11] J. Venkatramani, V. Nair, R. Sujith, S. Gupta, and S. Sarkar, Journal of Sound and Vibration **386**, 390 (2017).
[12] J. Venkatramani, S. Sarkar, and S. Gupta, Journal of Sound and Vibration **419**, 318 (2018).
[13] A. Raaj, J. Venkatramani, and S. Mondal, Chaos: An Interdisciplinary Journal of Nonlinear Science **29**, 043129 (2019).
[14] S. Boccaletti, J. Kurths, G. Osipov, D. Valladares, and C. Zhou, Physics reports **366**, 1 (2002).
[15] S. Mondal, S. Pawar, and R. Sujith, Chaos: An Interdisciplinary Journal of Nonlinear Science **27**, 103119 (2017).
[16] M. Aswathy and S. Sarkar, Journal of Sound and Vibration , 116230 (2021).
[17] C. Schäfer, M. G. Rosenblum, J. Kurths, and H.-H. Abel, Nature **392**, 239 (1998).
[18] C. Zhou, J. Kurths, I. Z. Kiss, and J. L. Hudson, Physical review letters **89**, 014101 (2002).
[19] A. Prasad, J. Kurths, S. K. Dana, and R. Ramaswamy, Physical Review E **74**, 035204 (2006).
[20] A. Prasad, S. K. Dana, R. Karnatak, J. Kurths, B. Blasius, and R. Ramaswamy, Chaos: An Interdisciplinary Journal of Nonlinear Science **18**, 023111 (2008).
[21] S. A. Pawar, A. Seshadri, V. R. Unni, and R. Sujith, Journal of Fluid Mechanics **827**, 664 (2017).
[22] S. Mondal, V. R. Unni, and R. Sujith, Journal of Fluid Mechanics **811**, 659 (2017).
[23] S. Mondal, S. A. Pawar, and R. Sujith, in *Energy for Propulsion* (Springer, 2018) pp. 125–150.
[24] S. A. Pawar, S. Mondal, N. B. George, and R. Sujith, in *2018 AIAA Aerospace Sciences Meeting* (2018) p. 0394.
[25] R. Mondal, C. Bose, and S. Mondal, in *Advances in Nonlinear Dynamics* (Springer, 2022) pp. 65–74.
[26] T. Hachijo, H. Gotoda, T. Nishizawa, and J. Kazawa, Physical Review Applied **14**, 014093 (2020).
[27] S. Vishal, A. Raaj, C. Bose, and J. Venkatramani, International Journal of Non-Linear Mechanics , 103766 (2021).
[28] M. G. Rosenblum, A. S. Pikovsky, and J. Kurths, Physical review letters **76**, 1804 (1996).
[29] M. G. Rosenblum, A. S. Pikovsky, and J. Kurths, Physical Review Letters **78**, 4193 (1997).
[30] V. Godavarthi, P. Kasthuri, S. Mondal, R. Sujith, N. Marwan, and J. Kurths, Chaos: An Interdisciplinary Journal of Nonlinear Science **30**, 033121 (2020).
[31] C. Zhou and J. Kurths, Physical review letters **88**, 230602 (2002).
[32] S. Dange, K. Manoj, S. Banerjee, S. A. Pawar, S. Mondal, and R. Sujith, Chaos: An Interdisciplinary Journal of Nonlinear Science **29**, 093135 (2019).
[33] A. Pikovsky, M. Rosenblum, and J. Kurths, "Synchronization: a universal concept in nonlinear science," (2002).
[34] A. Balanov, N. Janson, D. Postnov, and O. Sosnovtseva, *From simple to complex* (Springer, 2009).
[35] V. Nair and R. Sujith, Chaos: An Interdisciplinary Journal of Nonlinear Science **23**, 033136 (2013).
[36] J. Leishman and T. Beddoes, in *Proceedings of the 42nd Annual forum of the American Helicopter Society* (Washington DC, 1986) pp. 243–265.
[37] G. Dimitriadis, *Introduction to nonlinear aeroelasticity* (John Wiley & Sons, 2017).
[38] L. Goyaniuk, D. Poirel, and A. Benaissa, AIAA Journal **58**, 3286 (2020).
[39] D. Poirel and W. Yuan, Journal of Fluids and Structures **26**, 1174 (2010).
[40] H. Devathi and S. Sarkar, Computers & Structures **162**, 38 (2016).
[41] J. Venkatramani, S. Sarkar, and S. Gupta, Nonlinear Dynamics **92**, 1225 (2018).
[42] Y. Tang, J. Kurths, W. Lin, E. Ott, and L. Kocarev, Chaos: An Interdisciplinary Journal of Nonlinear Science **30**, 063151 (2020).